Zinc–Carboxylate Binding in Mixed Octadecanoic Acid and Octadecanol Monolayers on Proxy Seawater Solution Surfaces

Journal:	*ACS Earth and Space Chemistry*
Manuscript ID	sp-2021-00272k.R1
Manuscript Type:	Article
Date Submitted by the Author:	n/a
Complete List of Authors:	Auvil, Nicole; Ohio State University, Department of Chemistry and Biochemistry Vazquez de Vasquez, Maria; Ohio State University, Department of Chemistry and Biochemistry Allen, Heather; Ohio State University, Department of Chemistry and Biochemistry

Zinc–Carboxylate Binding in Mixed Octadecanoic Acid and Octadecanol Monolayers on Proxy Seawater Solution Surfaces

Authors: Nicole C. Auvil[a†], Maria G. Vazquez de Vasquez[a†], and Heather C. Allen*[a]

[a]Department of Chemistry & Biochemistry, The Ohio State University, 100 W. 18th Ave., Columbus OH 4321, USA.

†All authors contributed equally

*Correspondence: allen@chemisty.ohio-state.edu

Abstract

Organic coatings on sea spray aerosol are largely comprised of fatty acids in addition to a vast array of other organic molecules including fatty alcohols. The seawater from which sea spray aerosol originates contains metal ions that interact with the organic coating at the air-seawater interface, resulting in transport of these metals into the atmosphere. Metal binding within single-substance monolayers on aqueous solutions has been previously studied. However, such binding events within mixed monolayers, especially those of ocean relevant ratios, are not well explored. Here we examine four monolayer ratios of octadecanoic acid (stearic acid) to octadecanol (stearyl alcohol) on aqueous solutions with varying $ZnCl_2$ concentrations and a seawater-relevant NaCl concentration of 0.465 M. Surface pressure–area (Π-A) isotherms and infrared reflection-absorption spectroscopy (IRRAS) are used to quantify the Zn^{2+}–carboxylate surface binding affinities for each monolayer composition. We find that: Zn^{2+}–carboxylate binding is enhanced by ~300 times at the surface when compared to the bulk solution. Addition of 10% octadecanol reduces the apparent surface binding affinity by over 50% from 3.6×10^3 to 1.4×10^3 M^{-1}; this is significantly more than predicted from the slight reduction in viable 1:1 binding sites. Furthermore, 1:2 Zn^{2+}–carboxylate binding is shown to only be viable for the 100% and 95% fatty acid film whereas 1:1 binding is observed for all film ratios investigated.

Keywords

air-water interface, binding constant, surface spectroscopy, trace metal, metal ion enrichment, mixed monolayer, stearic acid, stearyl alcohol

Introduction

The air-water interface accommodates unique chemical and physical phenomena that can be significantly different than in the aqueous solution phase.[1–11] Surfactants, which are surface active molecules that possess both hydrophobic and hydrophilic characteristics, congregate in the interfacial region.[12] The air-water interface gives rise to preferred orientations of these surface active molecules such that the hydrophobic portion persists in the air phase and the hydrophilic portion interacts with the solution phase (i.e. the interfacial or subsurface water), thus minimizing the free energy of the surface.[13] Following this principle, water-soluble organic molecules generally gather at the ocean's surface to form a film called the sea surface microlayer (SSML); these molecules are then transferred from the SSML to sea spray aerosol during mechanical wave action and bubble bursting.[14,15]

Two important types of surfactant molecules naturally found in the SSML are fatty acids and fatty alcohols.[16–18] These molecules were recently discovered to exist in a nine to one ratio in oceanic emission samples.[19] Octadecanoic acid (OA, stearic acid, C18OOH), a C_{18} saturated fatty acid, is known to be enriched in sea spray aerosol, and octadecanol (OL, stearyl alcohol, C18OH) is its C_{18} saturated fatty alcohol analogue.[20,21] OA is often used as a proxy for the organic film on sea spray aerosol surfaces because it is the most prevalent oceanic fatty acid along with hexadecanoic acid (palmitic acid, C16OOH), both of which are derived from biogenic material including marine organisms.[22–24] An aim of this study is to emulate and observe the behavior of mixed monolayers containing OA and OL in ocean relevant ratios to provide insight on how film composition impacts metal-carboxylic acid binding and thus metal cation enrichment at the air-aqueous interface.

With an average concentration of 468 mM, Na^+ is the most concentrated metal ion in the ocean.[25] Zn^{2+} is known to have an average oceanic concentration of 6 nM and a high SSML enrichment factor relative to other oceanic metal ions despite its low concentration.[25,26] For scale, the total concentration of multivalent trace metals in the ocean is estimated to be about 164 nM.[25] Trace metal ions like Zn^{2+} have seawater concentrations many orders of magnitude lower than major metal ionic components like Na^+ and Mg^{2+}, yet have been found to be enriched in sea spray aerosol at significantly higher relative proportions.[25,27] Ion-surfactant interactions are hypothesized to cause this disparity in sea spray aerosol enrichment. Na^+ partakes in weak ionic interactions with surfactant headgroups.[28] Contrary to monovalent Na^+, multivalent metals have the ability to form strong ionic and, in some cases, covalent bonds with surfactant headgroups. Trace metals such as Zn^{2+} have previously been identified in the SSML at concentrations reaching one hundred times above those found in the subsurface bulk seawater, indicating significant enrichment factors.[26,29] When wave breaking or bubble bursting events occur, surfactant-bound trace metals can be transferred into sea spray aerosol.

Aspects of surfactant film structure including surface molecule orientation and packing can be altered by interactions with ions.[26,30,31] Previous studies have shown considerable ordering effects when divalent cations such as Zn^{2+} interact with a fatty acid film composed of OA, indicating strong binding and even metal-induced deprotonation of the -COOH group.[26,32,33] Monovalent Na^+, on the other hand, is not expected to interact as strongly with the carboxylate headgroup due to its smaller charge and larger ionic radius.[26,31] When compared to the metal complexation strength of OA, OL's binding affinity is assumed to be negligible due to its hydroxy headgroup.[26]

The primary goal of this study is to probe the effect of mixed monolayer composition on trace metal binding with monolayers composed of fatty acid and fatty alcohol molecules, typical components in SSML and sea spray aerosol. Mixed monolayers of OA and OL are thus systematically evaluated at four different ratios, and each ratio is studied on eight aqueous solutions of differing concentrations of $ZnCl_2$

while maintaining a constant and large NaCl ionic strength background equivalent to seawater NaCl concentrations.[26] Here, Zn^{2+} is chosen as the model trace metal due to its previously reported interaction strength with OA and its large enrichment factors in sea spray aerosol.[26,34] Infrared reflection–absorption spectroscopy (IRRAS) is used to probe these surface films and to quantify apparent surface binding constants using the integrated areas of carboxylate asymmetric stretch peaks as reporters.

Experimental

Materials and Sample Preparation

The materials used in this study were purchased commercially and used without further purification unless otherwise noted. Octadecanoic acid (OA, stearic acid, a C_{18} fatty acid, Sigma-Aldrich, ≥ 98.5% grade 1) and octadecanol (OL, stearyl alcohol, a C_{18} fatty alcohol, 99%, Sigma-Aldrich) were dissolved in chloroform (HPLC Grade, Fisher Scientific) to make ~3.8 mM OA and OL stock solutions. These solutions were combined in varying proportions to prepare ~3.8 mM mixed solutions at the ratios 100:0, 95:5, 90:10, and 85:15 OA:OL (w/w). Sodium chloride salt (NaCl) (99.999% trace metals basis, Aldrich, and 99.998% trace metals basis, Fisher Scientific) was baked in a furnace at 675°C for >8 hours to remove possible organic contamination. Zinc chloride salt ($ZnCl_2$) (99.999% trace metals basis, Aldrich) was used as purchased. NaCl and $ZnCl_2$ salt solutions were prepared using ultrapure water with a resistivity of 18.2 MΩ•cm (Milli-Q® Advantage A10, MilliporeSigma, Burlington, MA). The NaCl solution was filtered through Dionex OnGuard II M cartridges (Thermo Fisher Scientific) to remove possible trace metal impurities. NaCl and $ZnCl_2$ solutions are combined in the Langmuir trough to create the solution. The measured pH of the mixed salt solutions was 5.7 ± 0.15.

Surface Pressure – Area Isotherms

While Π-A isotherms were not directly used in the determination of Zn^{2+}–carboxylate surface binding constants, they were necessary for maintaining monolayer surface pressure during IRRAS scans and calibrating surfactant solution concentrations. Π-A isotherms were performed on a Teflon Langmuir trough with an area of 144.5 cm^2 fitted with movable Delrin barriers (KSV NIMA, Finland). Surface pressure was measured using custom cut filter paper Wilhelmy plates (ashless grade, Whatman). The trough and barriers were rigorously cleaned with reagent alcohol (Histological Grade, Fisher Scientific) and ultrapure water and dried before each trial. After the aqueous solution is added to the trough, its surface is checked for contamination by compressing the barriers and ensuring that the surface pressure does not rise above 0.2 mN/m. The surfactant solutions were deposited onto the surface dropwise with a microsyringe (Hamilton) to create the monolayer. The syringe was cleaned thoroughly between each trial with reagent alcohol, set to dry, and then rinsed ten times with chloroform (HPLC Grade, Fisher Scientific). The system was then left idle for ten minutes to allow for chloroform evaporation. The resulting monolayer was compressed at a constant rate of 5 mm/min per barrier until a surface pressure of 35 mN/m was achieved. To maintain this surface pressure, the barriers then moved back and forth synchronously at a slow rate of 1 mm/min. All experiments were repeated three times to ensure repeatability. The concentrations of the OA and OL stock solutions were calibrated to 24 and 21 $Å^2$/molecule, respectively.[35] All trials were run at 21 ± 1 °C and at a relative humidity of 31 ± 9%.

Infrared Reflection Absorption Spectroscopy

Infrared reflection-absorption spectroscopy (IRRAS) was the primary technique used to analyze Zn^{2+}–carboxylate binding. All IRRAS spectra were collected with a Fourier transform infrared (FTIR) spectrometer (Frontier, Perkin Elmer) equipped with an HgCdTe (MCT) detector that is cooled with liquid nitrogen. Within the spectrometer, the Langmuir trough sits on a breadboard alongside two planar gold-plated mirrors positioned such that the beam reflects off the monolayer at an incident angle of 48° relative to surface normal (**Figure 1 and Figure S1**). The incident unpolarized IR beam is reflected off the input gold mirror and onto the surface, where the beam interacts with the interface and is then reflected to the output mirror and finally to the detector. IRRAS scans were taken at 35 mN/m, a surface pressure at which the monolayer is in the untilted condensed phase. All spectra were collected immediately upon reaching the surface pressure of 35 mN/m.

IRRAS provides information about molecules at and near the air-water interface. Even though IRRAS is not explicitly surface-specific because infrared reflected light has a probe depth of a few μm, this technique is selective to probe surface monolayers due to ratioing of the reflectivity of the spread monolayer on the solution (R) to that of the spectral solution reflectivity (R_0).[36–41] The reflectance-absorbance (RA) is found using Equation 1 and is then plotted versus frequency.

$$RA = -log_{10}\left(\frac{R}{R_0}\right). \quad (1)$$

The analysis of RA data is based on spectral band frequency and intensity. Hydrocarbon chain conformation of the surfactants in the monolayer can be determined by evaluating the CH_2 symmetric and asymmetric stretching vibrational bands.[39] Additionally, the vibrational modes of the surfactant molecules' headgroups provide information about aqueous ion-surfactant binding interactions.[5,11,26,42] Surface binding affinities can be quantified via IRRAS using the techniques presented by Neal et al. and by Ariga.[5,11]

Each spectrum is an average of 400 scans in single beam mode with a resolution of 4 cm^{-1} within the range 4000-450 cm^{-1}. Data is plotted every 0.5 cm^{-1}. RA spectral baselines were corrected using a 4th order polynomial in the region of interest in addition to other minor data processing (OriginLab 9, Northampton, MA). All spectra shown here are averaged from at least three spectra using OriginPro 9's average function. The reported spectral uncertainties are considerable mostly due to spectral noise from insufficient or over subtraction of water vapor absorption. Humidity above the monolayer surface can be an issue, especially in the carboxylate region (**Figure S2**).[43,44] Given these interferences, note that for the 0, 10, and 25 mM Zn spectra in **Figure 3** and **Figure S3**, the water vapor line centered at 1559 cm^{-1} was removed as it obscured the band of interest. In addition, the sharp line centered at 1542 cm^{-1} in the 90:10 and 85:15 spectrum was removed for the same reason (see **Table S1** for values). Complete removal of gas phase water lines due to the high humidity of the lab air during acquisition days is nontrivial. Reported binding affinity errors incorporate both spectral and fitting uncertainties.

To determine the influence of monolayer composition on trace metal surface binding, surfactant headgroup-ion interactions were probed using surface-sensitive IRRAS in conjunction with Π-A isotherms (**Figure 1**). The OA:OL monolayer ratios examined were 100:0, 95:5, 90:10, and 85:15 (**Figure S4**). Each monolayer ratio was analyzed over aqueous solutions consisting of a constant NaCl background of 468 mM with eight varying $ZnCl_2$ concentrations between 0 and 25 mM. When the highest concentration of $ZnCl_2$ is included in the NaCl solution, the ionic strength increases to 543 mM. While the largest difference in molarity across all aqueous solutions is 25 mM, the difference in ionic strength is 75 mM due to the charge of the zinc ion. The molecular interaction of interest is the binding of divalent metal cations, Zn^{2+}, to the carboxylate headgroups within the monolayer. The intensity of the asymmetric carboxylate band at each concentration is normalized and fit to an adsorption curve to calculate the surface binding constant of Zn^{2+} at each ratio of fatty acid to fatty alcohol. This allows for quantitative comparison of binding between the four monolayer compositions.

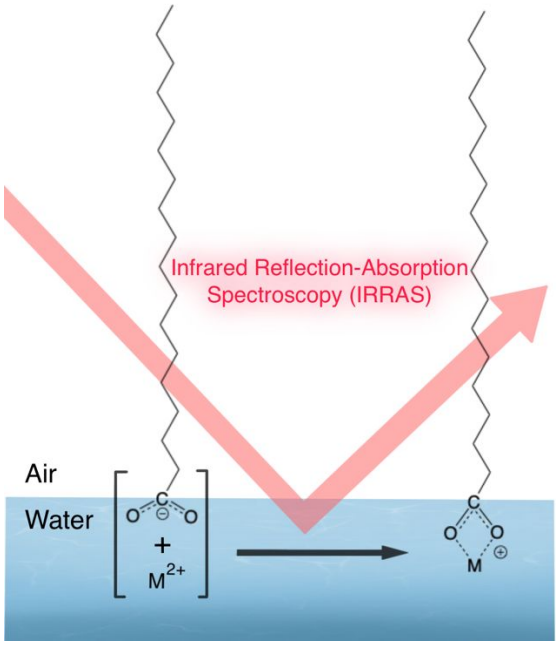

Figure 1. Carboxylate-metal binding at the air-water interface is probed using IRRAS.

Results and Discussion

A pure monolayer is composed of only one type of surfactant at the air-water interface, whereas a mixed monolayer contains a combination of two or more surfactants.[45] Due to the immense diversity in sources from which atmospheric and oceanic organic molecules originate, mixed monolayer films are more suitable for the purpose of representing sea spray aerosol and the SSML. Experimental techniques and molecular dynamics simulations have both been used to study the interfacial properties of mixed monolayers at the air-water interface.[22,46,47] Surface properties of binary mixtures of fatty acids with other organic molecules such as amines, esters, cholesterols, and alcohols have received significant attention during the past two decades.[46,48,49] These studies have revealed substantial differences between the physical and chemical properties of a pure fatty acid monolayer and a mixed monolayer that contains fatty acid. The inclusion of a secondary surfactant in a fatty acid monolayer has been shown to alter film packing structure[22], thermodynamic behavior[49], and monolayer stability.[46] Despite the considerable impact monolayer composition can have on film structure and stability, single-component monolayer

studies dominate the field.[24,26,28,30–32,42,50–54] To the author's knowledge, no previous studies have investigated how monolayer composition impacts trace metal surface enrichment.

While the complexity of mixed monolayers allows for better representation of real-world systems, it also creates experimental challenges. One challenge is the physical creation of a mixed monolayer. Immiscibility of two or more surfactants can create two-dimensional domains, which are island-like structures on the water's surface. This is in contrast to a miscible film in which two or more types of surfactants mix to form an ideal homogenous film.[45] In 2015, Lee et al. conducted a study to determine the best method for creating a homogenously mixed multi-component monolayer that contained OA and other surfactants.[55] Lee et al. found that the main factor in monolayer mixing is the spreading method used in preparing the monolayer. When OA and the other surfactant are prepared in separate organic solutions and spread individually onto the aqueous solution, the two surfactants cannot mix well, resulting in distinct domain formation.[55] However, when OA and the other surfactants are pre-mixed in the solvent prior to spreading on the aqueous solution, a well-mixed monolayer is formed.[55]

All monolayers in this study were compressed and held at a surface pressure of 35 mN/m with an approximate mean molecular area of 21.5 $Å^2$/molecule while IRRAS scans were taken. At this surface pressure, a monolayer of OA on a zinc-containing solution exists in the highly ordered untitled condensed phase.[42] While this system is not at equilibrium, the highly ordered metastable state may be more representative of atmospheric and ocean films in nature. Dynamic wave oscillation at the ocean's surface and the shrinking of sea spray aerosol particles in the atmosphere due to evaporation can cause surface films to expand and condense, resulting in deviation from the equilibrium state. Because these film perturbations are ubiquitous in moving or turbulent water, a non-equilibrium system is suitable for their emulation. Additionally, fatty acid molecules such as OA have been found to form complex three-dimensional aggregates at the air-water interface under certain conditions, disrupting the two-dimensional monolayer structure.[56] The high surface pressure and ionic strength used in this study may

play a role in inhibiting the formation of these aggregates, thus stabilizing the monolayer throughout measurement.[51]

IRRAS spectra in the alkyl region of OA:OL mixed monolayers spread on solutions of 25 mM $ZnCl_2$ and 468 mM NaCl are shown in **Figure 2.** Here, the methylene asymmetric stretch ($\nu_{as}(CH_2)$) is found at 2918 cm^{-1} and the methylene symmetric stretch ($\nu_s(CH_2)$) is found at 2851 cm^{-1}. The positions of these two modes indicate that the monolayer's hydrocarbon tails take an all-trans conformation.[30,39,42,57] These vibrational modes are located at the same wavenumbers for all concentrations of zinc **(Figure S5**), conveying that the presence of zinc does not impact hydrocarbon tail ordering. Additionally, the intensities of the modes in **Figure 2** are equal across all four monolayer compositions, indicating mixed monolayers of different OA:OL ratios have equal alkyl chain surface concentrations.

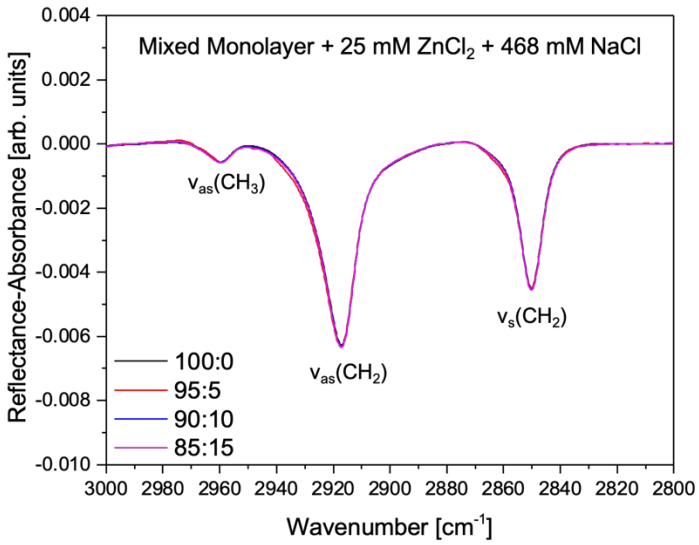

Figure 2. Alkyl region of IRRAS spectra of each monolayer composition (OA:OL) on an aqueous solution of 25 mM $ZnCl_2$ and 468 mM NaCl at a surface pressure of 35 mN/m.

While there is no apparent variation between the alkyl regions of the four monolayer compositions in **Figure 2,** there are large spectral differences in the carboxylate region when each

monolayer composition is analyzed on a range of aqueous $ZnCl_2$ solution concentrations (**Figure S3**). All spectra have had the aqueous solution background spectrum subtracted and therefore contain information specific to the monolayer film. The full set of IRRAS spectra was utilized to study Zn^{2+}-carboxylate surface binding at the air-water interface. Here in **Figure 3**, we show a representative set of these spectra. The location of the methylene scissoring band ($\delta(CH_2)$) at 1469 cm^{-1} confirms that the hydrocarbon chains are packed in a hexagonal subcell structure.[58] The spectra also reveal the carbonyl stretch (ν(C=O)) at 1729 cm^{-1}, the carboxylate symmetric stretch ($\nu_s(COO^-)$) at 1404 cm^{-1}, and the

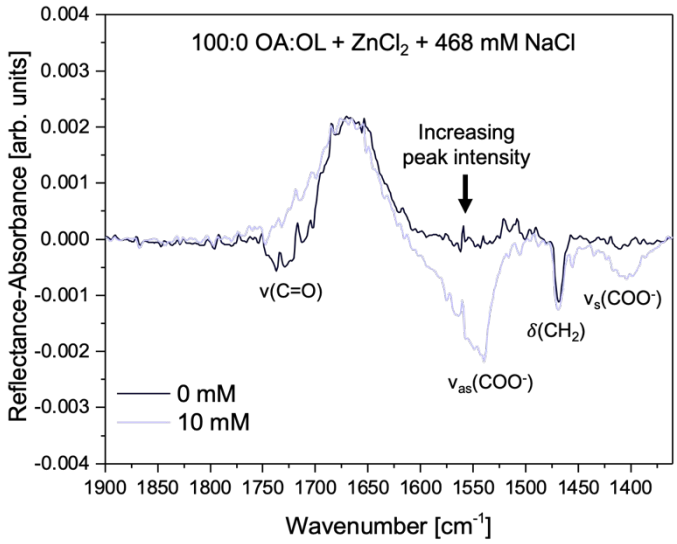

Figure 3. Carboxylate region of IRRAS spectra of the 100:0 OA:OL mixed monolayer on an aqueous solution containing 468 mM NaCl, a variable amount of $ZnCl_2$, and held at a surface pressure of 35 mN/m. Some water vapor lines removed for clarity (**Table S1**).

carboxylate asymmetric stretch ($\nu_{as}(COO^-)$) at 1546 cm^{-1}. These values are consistent with previous studies.[32,42] It is seen across all monolayer compositions that the $\nu_{as}(COO^-)$ mode increases in area and intensity with increasing zinc concentration. This pattern is indicative of binding interaction between Zn^{2+} and the carboxylate headgroup of OA. In addition, the disappearance of the ν(C=O) mode with increasing zinc concentration indicates that the Zn^{2+}–carboxylate binding interaction is primarily nonsymmetric

bidentate chelation, although contributions due to other binding geometries are possible. Because the carboxylate stretching mode displays sensitivity to binding, it is used as a probe of Zn^{2+}–carboxylate binding interactions across monolayer compositions.[5,32,42,50]

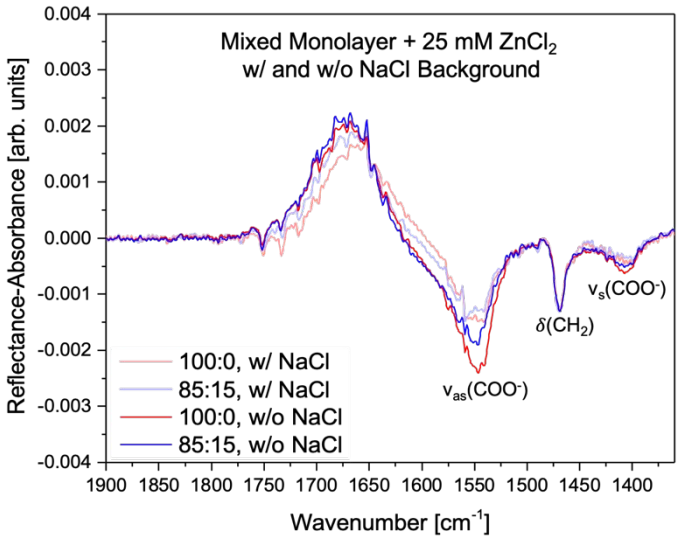

Figure 4. Carboxylate region of IRRAS spectra of the 100:0 and 85:15 OA:OL mixed monolayer compositions on aqueous solutions containing either 0 mM or 468 mM NaCl, 25 mM $ZnCl_2$, and held at a surface pressure of 35 mN/m.

Prior to evaluation of the specific effect of the mixed monolayer on binding and given the large concentrations of NaCl used in these studies as a proxy for ocean SSML and sea spray aerosol solutions, we tested the effect of NaCl. As shown in **Figure 4**, the spectra without NaCl have $\nu_{as}(COO^-)$ modes that are larger in intensity, which is indicative of an increase zinc–OA binding interactions. It is believed that the large ionic strength from the oceanic concentrations of NaCl interfere with the binding efficiency of Zn^{2+} due to ionic shielding. All other experiments in this study have an aqueous solution that contains oceanic levels of NaCl, resulting in an accurate emulation of binding conditions at the SSML and in sea spray aerosol films.

Now that the effect of NaCl is established, we examine the impact of incorporating OL into an OA monolayer film. When an OA monolayer is diluted with OL, the $\nu_{as}(COO^-)$ mode changes in area which allows for evaluation of Zn^{2+}–carboxylate binding. To compare the $\nu_{as}(COO^-)$ modes across all monolayer ratios and zinc concentrations, the peak areas were determined via integration and compiled into **Figure 5.** At low $ZnCl_2$ concentrations, it is observed that peak areas do not vary significantly between monolayer compositions. However, they do at higher $ZnCl_2$ concentrations; the $\nu_{as}(COO^-)$ peak areas decrease with increasing amounts of OL in the monolayer, most significantly in the 90:10 and 85:15 OA:OL monolayers. This pattern can be observed for the highest $ZnCl_2$ concentration spectra in **Figure S6**. Because the $\nu_{as}(COO^-)$ mode is sensitive to binding interactions, this analysis suggests that (1) there is a general increase in binding with an increase in zinc concentration, and (2) there is relatively no change in binding across the OA:OL ratios except with the higher concentrations of zinc. This latter point is somewhat surprising given that the concentration of the carboxylate is decreasing with decreasing amount of OA in the monolayer.

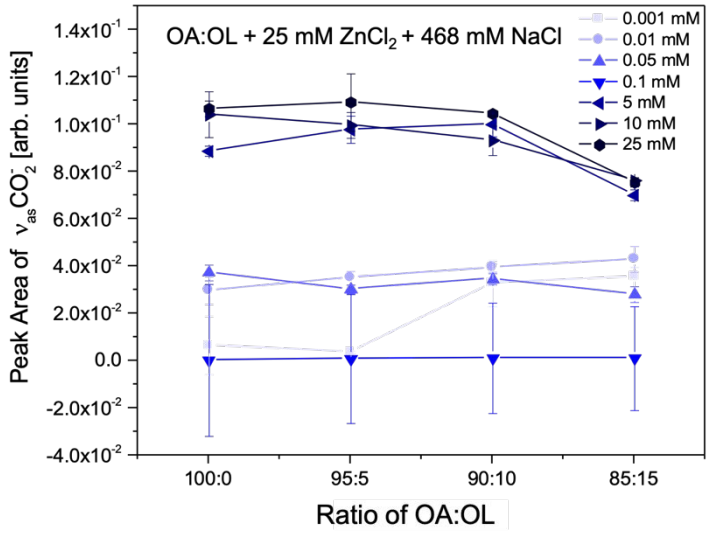

Figure 5. Integrated total peak area of the $\nu_{as}(COO^-)$ mode (1490-1610 cm^{-1}) displayed for each aqueous $ZnCl_2$ concentration across all monolayer compositions. Error bars correspond to one standard deviation.

Determining Surface Binding Affinity

Table 1. Normalized carboxylate asymmetric peak areas for each zinc concentration and monolayer composition.

	Normalized $v_{as}(COO^-)$ Peak Area			
Zn^{2+} Concentration (mM)	100:0	95:5	90:10	85:15
0	0	0	0	0
0.001	-0.072 ± 0.143	-0.063 ± 0.039	0.118 ± 0.127	0.321 ± 0.074
0.01	0.179 ± 0.085	0.253 ± 0.058	0.201 ± 0.054	0.449 ± 0.093
0.05	0.260 ± 0.069	0.205 ± 0.049	0.141 ± 0.056	0.198 ± 0.059
0.1	0.205 ± 0.063	0.176 ± 0.050	0.002 ± 0.063	0.093 ± 0.033
5	0.808 ± 0.081	0.884 ± 0.132	0.945 ± 0.093	0.907 ± 0.052
10	0.974 ± 0.134	0.902 ± 0.132	0.860 ± 0.099	1.012 ± 0.044
25	1.000 ± 0.094	1.000 ± 0.179	1.000 ± 0.069	1.000 ± 0.051

To quantify the binding efficiencies of each monolayer and the impact of film heterogeneity, binding affinities were determined based on the asymmetric carboxylate stretch peak area. The peak areas, shown in **Table 1**, were quantified via peak integration, and normalized via min-max normalization, meaning that a value of 0 corresponds to the peak area on a solution of 0 mM $ZnCl_2$ and 468 mM NaCl and a value of 1 corresponds to the peak area on a solution of 25 mM $ZnCl_2$, 468 mM NaCl. The reported errors correspond to one standard deviation that has been propagated through the operations used in the normalization calculation. Since the minimum value is normalized to the peak area of a system containing only the background NaCl and no $ZnCl_2$, the binding indicated by these peak areas is assumed to be solely due to Zn^{2+}–carboxylate interactions.

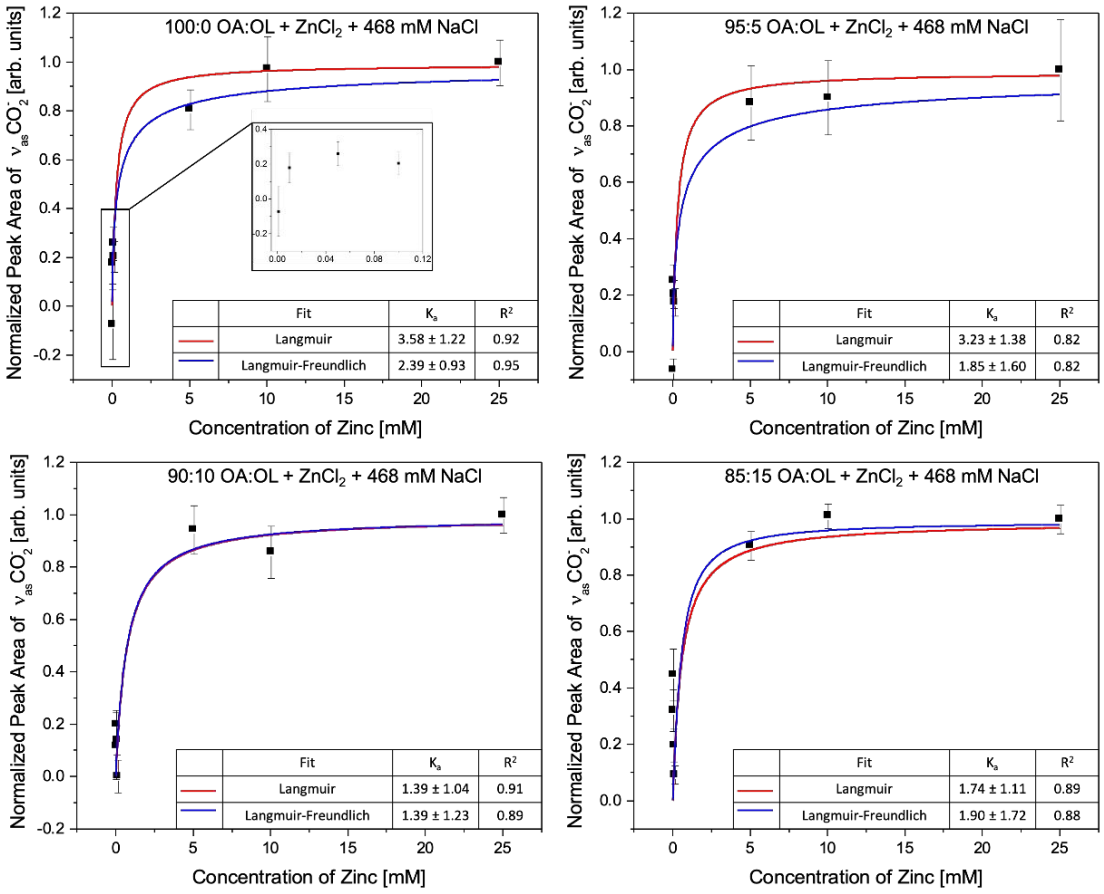

Figure 6. Normalized peak area of $\nu_{as}(COO^-)$ of OA:OL mixed monolayers in the ratios 100:0 (top left) with inset showing low concentration regime, 95:5 (top right), 90:10 (bottom left), and 85:15 (bottom right). All scans have an aqueous solution containing 468 mM NaCl, a variable amount of $ZnCl_2$, and a surface pressure of 35 mN/m. Surface binding affinities found by each adsorption model are given as mM^{-1}. Error bars correspond to one standard deviation that has been propagated through the operations used in the normalization calculation.

Results are plotted in **Figure 6** as concentration of zinc versus normalized peak area of $\nu_{as}(COO^-)$, separated by monolayer composition. All four monolayer compositions show positive correlation between peak area and zinc concentration. The plots are fit to two different surface adsorption models, Langmuir and Langmuir-Freundlich (Equations 2, 3)

Langmuir $$A = A_{max}\frac{K_a[Zn^{2+}]}{K_a[Zn^{2+}]+1} \quad (2)$$

Langmuir-Freundlich $$A = A_{max}\frac{[K_a[Zn^{2+}]]^n}{[K_a[Zn^{2+}]]^n+1} \quad (3)$$

where A and A_{max} are peak intensity and maximum peak intensity of $\nu_{as}(COO^-)$, $[Zn^{2+}]$ is the solution concentration of zinc, n is an empirical constant, and K_a is the affinity constant for adsorption which is defined as the inverse of the dissociation constant.[5,59–61] For both adsorption models, the binding is assumed to occur at a 1:1 ratio of zinc to OA. Based on R^2 value, the Langmuir-Freundlich model provides the most precise fit for 100:0, while the Langmuir model provides the most precise fit for 90:10 and 85:15. The two adsorption models result in an equally precise fit for 85:15. Across all monolayer compositions, differences in quality of fit between the two models are minimal.

The Langmuir adsorption model is a well-accepted method for quantifying how an adsorbate forms a layer on a given surface based on the equilibrium of ions between the two phases.[62–64] Because of the simplifications in the Langmuir model, modifications have been developed to create more complex models.[61] The Langmuir-Freundlich adsorption model is one such equation. It includes an exponential term and an empirical constant, n, which was used by Soares et al. to describe surface adsorption on heterogeneous surfaces.[61,64] This feature can be useful for analyzing adsorption on non-uniform surfaces, such as a mixed OA:OL monolayer. The exponential term of the Langmuir-Freundlich model provides an additional parameter in comparison to the Langmuir model, which should result in Langmuir-Freundlich producing a more precise fit. However, the Langmuir-Freundlich model produced a less precise fit for ¾ of the ratios studied. In addition, the exponential term is supposed to describe surface heterogeneity such that it would equal 1 for 100:0 (a homogeneous system), resulting in no difference between the Langmuir and Langmuir-Freundlich fits. However, the two models do not produce equal curves for this ratio. The

additional parameter in the Langmuir-Freundlich model proved to be less than optimal for representing the physical aspect of surface heterogeneity and improving model precision. Because of this, we report and analyze the binding affinity K_a values derived only from the Langmuir adsorption model (**Figure 7)**.

In general, we observe that an increase in the concentration of OL decreases the overall binding affinity of the monolayer, that is, of the carboxylic acid headgroup. For example, for the 90:10 and 85:15 compositions, we would expect a 10 and 15% drop in binding affinity given there is a 10 and 15% lower concentration of OA in the monolayer when compared to 100:0. Yet a ~50% reduction in binding affinity is observed, leading us to the conclusion that the alcohol headgroup of the OL reduces the ability of the carboxylic acid headgroup to efficiently bind. This can be simply explained such that the OH of the alcohol perturbs the carboxylic acid and carboxylate intermolecular hydrogen bonding.

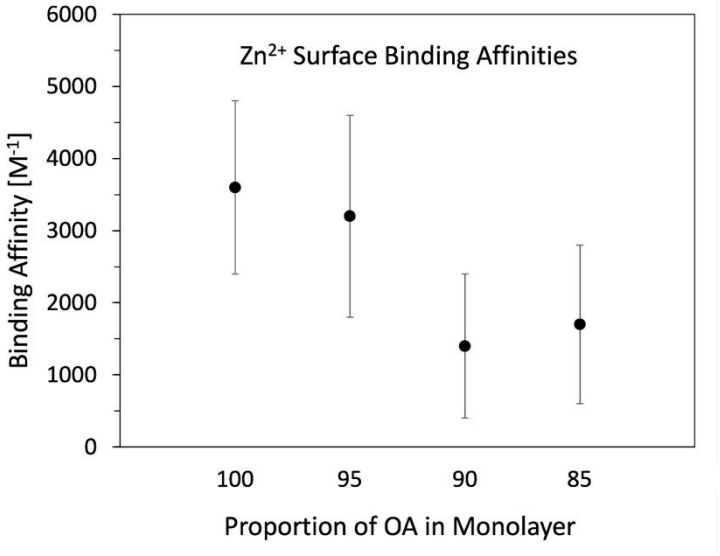

OA:OL Ratio	Binding Affinity (M^{-1})
100:0	$3.6\ (1.2) \times 10^3$
95:5	$3.2\ (1.4) \times 10^3$
90:10	$1.4\ (1.0) \times 10^3$
85:15	$1.7\ (1.1) \times 10^3$

Figure 7. Summary of the binding affinities of Zn^{2+} for each of the four reported monolayer compositions. A 1:1 Zn^{2+}:carboxylate binding is assumed. The error values given in parentheses correspond to one standard deviation that has been propagated through the operations used in the normalization calculation.

The Stoichiometry of Complex Formation. As stated previously, all reported binding information assumes 1:1 Zn^{2+}–carboxylate complexation at the air-water interface. However, this may not be an

electrostatically preferred system because the Zn^{2+} ion has a divalent positive charge while the carboxylate group has a monovalent negative charge, meaning that the 1:1 complex would carry a 1+ charge. A 1:2 Zn^{2+}–carboxylate complex, moreover, would carry an overall charge of zero. One proposed mechanism for the formation of the 1:2 complex is a ternary single-step reaction in which the aqueous zinc ion and two free, adjacent carboxylate headgroups bind together synchronously (Equation 4).[65]

$$K_{a1}[Zn^{2+}][OA^{-}]^2 = [Zn(OA)_2] \quad (4)$$

$$A = A_{max}\frac{1 + 8K_{a1}[S][Zn^{2+}] - \sqrt{1 + 16K_{a1}[S][Zn^{2+}]}}{8K_{a1}[S][Zn^{2+}]} \quad (5)$$

The 1:2 complexation single-step adsorption model is given as Equation 5, where $K_{a1}[S]$ is the binding parameter of the single-step reaction and [S] specifically is the density of surface binding sites. When applied to the IRRAS data, this adsorption model provides a poor fit with low R^2 values. The poor fit may be due to the fact that ternary reactions are not kinetically favorable and are unlikely to occur spontaneously. Therefore, this ternary mechanism of binding will not be considered further.

Another proposed mechanism for the formation of the 1:2 Zn^{2+}–carboxylate complex is a two-step process. In the first step, which is bimolecular, a zinc ion binds to a single carboxylate headgroup to form a 1:1 Zn^{2+}–carboxylate complex (Equation 6). In the second step, an adjacent and free carboxylate headgroup binds to the existing complex to form a zinc ion bound by two carboxylate headgroups (Equation 7).[65]

Step 1: $$K_a[Zn^{2+}][OA^{-}] = [Zn(OA)]^{+} \quad (6)$$

Step 2: $$K_b[OA^{-}][Zn(OA)]^{+} = [Zn(OA)_2] \quad (7)$$

$$A = A_{max}\frac{1 + 8K_b[S]K_a[Zn^{2+}] - (K_a[Zn^{2+}])^2 + (K_a[Zn^{2+}] - 1)\cdot\sqrt{(K_a[Zn^{2+}] + 1)^2 + 16K_b[S]K_a[Zn^{2+}]}}{16K_b[S]K_a[Zn^{2+}]} \quad (8)$$

The 1:2 complexation two-step adsorption model is given in Equation 8, where $K_b[S]$ is the binding parameter of Step 2 and [S] is the density of surface binding sites.[65] Step 1 is equal to the 1:1 binding mechanism assumed for the previously calculated Langmuir adsorption, and therefore K_a here is equal to the K_a found by Langmuir fitting.[65] Since K_a in the two-step equation is equal to the Langmuir binding constant, $K_b[S]$ is a parameter that is indicative of any 1:2 binding above and beyond the binding achieved in Step 1.[65] The two-step adsorption model fits the data much more precisely than the single-step model. For each ratio of OA:OL, the two-step adsorption curve consistently falls between the Langmuir curve and the Langmuir-Freundlich curve, with R^2 values in the same range. Values from the fit are given in **Figure 8**.

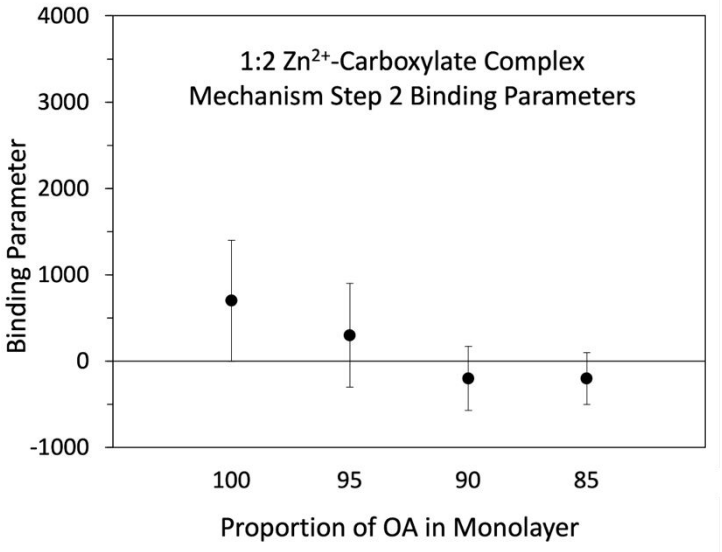

OA:OL Ratio	Binding Parameter
100:0	0.7 (0.7) × 10^3
95:5	0.3 (0.6) × 10^3
90:10	-0.2 (0.4) × 10^3
85:15	-0.2 (0.3) × 10^3

Figure 8. Summary of the binding parameters for Step 2 in the mechanism of 1:2 Zn^{2+}–carboxylate complex formation for each of the four reported monolayer compositions. The error values given in parentheses correspond to one standard deviation that has been propagated through the operations used in the normalization calculation.

The trend in binding parameters reveals that when there is a higher proportion of OA in the monolayer, 1:1 surface complexes are more likely to complete Step 2 of the mechanism to become 1:2

Zn^{2+}–carboxylate complexes. This trend is kinetically viable because as the OA monolayer is diluted with OL, there is a decreased probability that any given molecule adjacent to a 1:1 complex is OA. When there are less adjacent OA molecules available, it may be more energetically taxing for the 1:1 complex to bind another carboxylate headgroup. A schematic of this motif is presented in **Figure 9**. There is a distinct divide in binding parameter value between the upper two and the lower two OA:OL ratios: the upper two are positive, while the lower two are negative. This may indicate that at some point between the 95:5 and 90:10, the proportion of OL in the monolayer becomes too high to support significant 1:2 Zn^{2+}–carboxylate complex formation.

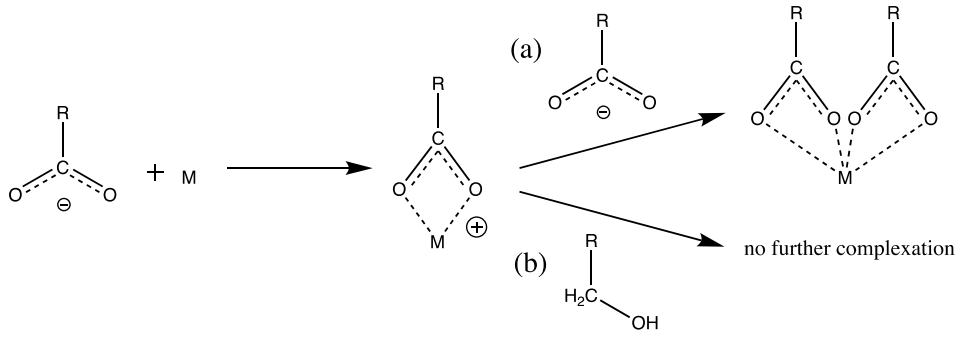

Figure 9. Proposed motif of mechanism Step 2 in the two-step formation of the 1:2 Zn^{2+}–carboxylate complex at the air-water interface. M represents divalent Zn^{2+}. (a) A monolayer environment rich in OA is conducive to successful completion of Step 2, but as the proportion of OL increases (b) the likelihood of Step 2 completion is diminished.

Conclusion

Mixed monolayers, as opposed to single component monolayers, are more representative of real-world atmospheric and oceanic systems, particularly for evaluating metal surface enrichment and binding. Here Zn^{2+}–carboxylate surface binding was probed as a function of octadecanoic acid to octadecanol monolayer composition using surface pressure isotherms and infrared reflection spectroscopy. All systems were evaluated with a surface pressure of 35 mN/m, a mean molecular area of approximately 21.5 $Å^2$/molecule, and an untilted condensed monolayer structure. Surface binding affinities for 1:1 Zn^{2+}–

carboxylate surface complexes were found for each of the four ratios of octadecanoic acid to octadecanol studied (100:0, 95:5, 90:10, and 85:15) via Langmuir adsorption model. All 1:1 Zn^{2+}–carboxylate surface binding affinities were found to be on the order of 10^3, which is about 300 times stronger than the analogous bulk binding process, indicating enhanced binding at the interface. Monolayer composition was found to influence trace metal surface binding affinity; the addition of octadecanol in a monolayer of octadecanoic acid disproportionately reduced Zn^{2+}–carboxylate surface binding. This may be because the alcohol headgroup of octadecanol reduced the ability of the carboxylic acid headgroup to efficiently bind. Finally, the potential of each system to form 1:2 Zn^{2+}–carboxylate surface complexes was analyzed using a bivalent binding model. It was found that the two highest monolayer ratios, 100:0 and 95:5, can support formation of 1:2 Zn^{2+}–carboxylate surface complexes via a two-step reaction mechanism. Results reveal that ratios similar to those found in the sea surface microlayer and in sea spray aerosol films of octadecanoic acid and octadecanol impact surface binding affinity of Zn^{2+}, an oceanic trace metal.

Author Information:

Corresponding Author

Heather C. Allen − Department of Chemistry & Biochemistry, The Ohio State University, Columbus, Ohio 43210, United States; orcid.org/0000-0003-3120-6784; Phone: +1-614-292-4707; Email: allen@chemistry.ohio-state.edu; Fax: +1- 614-292-1685

Authors

Nicole Auvil − Department of Chemistry & Biochemistry, The Ohio State University, Columbus, Ohio 43210, United States

Maria Vazquez de Vasquez − Department of Chemistry & Biochemistry, The Ohio State University, Columbus, Ohio 43210, United States

Author Contributions: N.C.A and M.G.V.V. contributed equally to this work. H.C.A supervised the project and edited the manuscript.

Conflict of Interest: The authors declare no conflicts of interest.

Acknowledgements: Funding for this research was provided by the National Science Foundation Center for Aerosols Impacts on the Chemistry of the Environment (NSF-CAICE) under Grant No. CHE-1801971. The authors acknowledge NIST Chemistry WebBook for providing useful spectral data. The authors declare no competing financial interest. We thank Jennifer F. Neal for assistance with adsorption curve fitting and insightful discussions. We also thank Kimberly A. Carter-Fenk for helpful discussions.

Supporting Information Avaliable: The supporting information is available free to charge at <website> at DOI:<>

Experimental setup images featuring the Langmuir trough and custom-build IRRAS, schematic diagram of mixed monolayer systems, water vapor spectrum adapted from NIST Chemistry WebBook, carboxylate and alkyl regions of IRRAS spectra of OA:OL mixed monolayers, list of water vapor lines removed from spectra for clarity.

Data used to produce figures and conclusions in this manuscript are included in the Center for Aerosol Impacts on the Chemistry of the Environment (CAICE) data set hosted by the UCSD Library Digital Collections<website>

References

(1) Murdachaew, G.; Varner, M. E.; Phillips, L. F.; Finlayson-Pitts, B. J.; Gerber, R. B. Nitrogen Dioxide at the Air–Water Interface: Trapping, Absorption, and Solvation in the Bulk and at the Surface. *Phys. Chem. Chem. Phys.* **2012**, *15* (1), 204–212. https://doi.org/10.1039/C2CP42810E.

(2) Tinel, L.; Rossignol, S.; Bianco, A.; Passananti, M.; Perrier, S.; Wang, X.; Brigante, M.; Donaldson, D. J.; George, C. Mechanistic Insights on the Photosensitized Chemistry of a Fatty Acid at the Air/Water Interface. *Environ. Sci. Technol.* **2016**, *50* (20), 11041–11048. https://doi.org/10.1021/acs.est.6b03165.

(3) Nissenson, P.; Dabdub, D.; Das, R.; Maurino, V.; Minero, C.; Vione, D. Evidence of the Water-Cage Effect on the Photolysis of NO3− and FeOH2+. Implications of This Effect and of H2O2 Surface Accumulation on Photochemistry at the Air–Water Interface of Atmospheric Droplets. *Atmos. Environ.* **2010**, *44* (38), 4859–4866. https://doi.org/10.1016/j.atmosenv.2010.08.035.

(4) Kusaka, R.; Nihonyanagi, S.; Tahara, T. The Photochemical Reaction of Phenol Becomes Ultrafast at the Air–Water Interface. *Nat. Chem.* **2021**, *13* (4), 306–311. https://doi.org/10.1038/s41557-020-00619-5.

(5) Neal, J. F.; Zhao, W.; Grooms, A. J.; Flood, A. H.; Allen, H. C. Arginine–Phosphate Recognition Enhanced in Phospholipid Monolayers at Aqueous Interfaces. *J. Phys. Chem. C* **2018**, *122* (46), 26362–26371. https://doi.org/10.1021/acs.jpcc.8b03531.

(6) Rogers, M. M.; Neal, J. F.; Saha, A.; Algarni, A. S.; Hill, T. C. J.; Allen, H. C. The Ocean's Elevator: Evolution of the Air–Seawater Interface during a Small-Scale Algal Bloom. *ACS Earth Space Chem.* **2020**, *4* (12), 2347–2357. https://doi.org/10.1021/acsearthspacechem.0c00239.

(7) Van Loon, L. L.; Allen, H. C. Uptake and Surface Reaction of Methanol by Sulfuric Acid Solutions Investigated by Vibrational Sum Frequency Generation and Raman Spectroscopies. *J. Phys. Chem. A* **2008**, *112* (34), 7873–7880. https://doi.org/10.1021/jp712134s.

(8) Finlayson-Pitts, B. J. Reactions at Surfaces in the Atmosphere: Integration of Experiments and Theory as Necessary (but Not Necessarily Sufficient) for Predicting the Physical Chemistry of Aerosols. *Phys. Chem. Chem. Phys.* **2009**, *11* (36), 7760–7779. https://doi.org/10.1039/B906540G.

(9) Sakurai, M.; Tamagawa, H.; Inoue, Y.; Ariga, K.; Kunitake, T. Theoretical Study of Intermolecular Interaction at the Lipid−Water Interface. 1. Quantum Chemical Analysis Using a Reaction Field Theory. *J. Phys. Chem. B* **1997**, *101* (24), 4810–4816. https://doi.org/10.1021/jp9700591.

(10) Tamagawa, H.; Sakurai, M.; Inoue, Y.; Ariga, K.; Kunitake, T. Theoretical Study of Intermolecular Interaction at the Lipid−Water Interface. 2. Analysis Based on the Poisson−Boltzmann Equation. *J. Phys. Chem. B* **1997**, *101* (24), 4817–4825. https://doi.org/10.1021/jp9700600.

(11) Ariga, K. Molecular Recognition at the Air–Water Interface: Nanoarchitectonic Design and Physicochemical Understanding. *Phys. Chem. Chem. Phys.* **2020**, *22* (43), 24856–24869. https://doi.org/10.1039/D0CP04174B.

(12) Characteristic Features of Surfactants. In *Surfactants and Interfacial Phenomena*; John Wiley & Sons, Ltd, 2012; pp 1–38. https://doi.org/10.1002/9781118228920.ch1.

(13) Donaldson, D. J.; Vaida, V. The Influence of Organic Films at the Air−Aqueous Boundary on Atmospheric Processes. *Chem. Rev.* **2006**, *106* (4), 1445–1461. https://doi.org/10.1021/cr040367c.

(14) Cochran, R. E.; Jayarathne, T.; Stone, E. A.; Grassian, V. H. Selectivity Across the Interface: A Test of Surface Activity in the Composition of Organic-Enriched Aerosols from Bubble Bursting. *J. Phys. Chem. Lett.* **2016**, *7* (9), 1692–1696. https://doi.org/10.1021/acs.jpclett.6b00489.

(15) Resch, F.; Afeti, G. Film Drop Distributions from Bubbles Bursting in Seawater. *J. Geophys. Res. Oceans* **1991**, *96* (C6), 10681–10688. https://doi.org/10.1029/91JC00433.

(16) Alpert, P. A.; Ciuraru, R.; Rossignol, S.; Passananti, M.; Tinel, L.; Perrier, S.; Dupart, Y.; Steimer, S. S.; Ammann, M.; Donaldson, D. J.; George, C. Fatty Acid Surfactant Photochemistry Results in New Particle Formation. *Sci. Rep.* **2017**, *7* (1), 12693. https://doi.org/10.1038/s41598-017-12601-2.

(17) Cochran, R. E.; Laskina, O.; Jayarathne, T.; Laskin, A.; Laskin, J.; Lin, P.; Sultana, C.; Lee, C.; Moore, K. A.; Cappa, C. D.; Bertram, T. H.; Prather, K. A.; Grassian, V. H.; Stone, E. A. Analysis of Organic Anionic Surfactants in Fine and Coarse Fractions of Freshly Emitted Sea Spray Aerosol. *Environ. Sci. Technol.* **2016**, *50* (5), 2477–2486. https://doi.org/10.1021/acs.est.5b04053.

(18) Lin, J.; Dai, Q.; Zhao, H.; Cao, H.; Wang, T.; Wang, G.; Chen, C. Photoinduced Release of Volatile Organic Compounds from Fatty Alcohols at the Air–Water Interface: The Role of Singlet Oxygen Photosensitized by a Carbonyl Group. *Environ. Sci. Technol.* **2021**, *55* (13), 8683–8690. https://doi.org/10.1021/acs.est.1c00313.

(19) Perkins, R. J.; Vazquez de Vasquez, M. G.; Beasley, E. E.; Hill, T. C. J.; Stone, E. A.; Allen, H. C.; DeMott, P. J. Relating Structure and Ice Nucleation of Mixed Surfactant Systems Relevant to Sea Spray Aerosol. *J. Phys. Chem. A* **2020**, *124* (42), 8806–8821. https://doi.org/10.1021/acs.jpca.0c05849.

(20) Ellison, G. B.; Tuck, A. F.; Vaida, V. Atmospheric Processing of Organic Aerosols. *J. Geophys. Res. Atmospheres* **1999**, *104* (D9), 11633–11641. https://doi.org/10.1029/1999JD900073.

(21) Rouvière, A.; Ammann, M. The Effect of Fatty Acid Surfactants on the Uptake of Ozone to Aqueous Halogenide Particles. *Atmospheric Chem. Phys.* **2010**, *10* (23), 11489–11500. https://doi.org/10.5194/acp-10-11489-2010.

(22) Griffith, E. C.; Adams, E. M.; Allen, H. C.; Vaida, V. Hydrophobic Collapse of a Stearic Acid Film by Adsorbed L-Phenylalanine at the Air–Water Interface. *J. Phys. Chem. B* **2012**, *116* (27), 7849–7857. https://doi.org/10.1021/jp303913e.

(23) Cheng, S.; Li, S.; Tsona, N. T.; George, C.; Du, L. Insights into the Headgroup and Chain Length Dependence of Surface Characteristics of Organic-Coated Sea Spray Aerosols. *ACS Earth Space Chem.* **2019**, *3* (4), 571–580. https://doi.org/10.1021/acsearthspacechem.8b00212.

(24) Li, S.; Du, L.; Wei, Z.; Wang, W. Aqueous-Phase Aerosols on the Air-Water Interface: Response of Fatty Acid Langmuir Monolayers to Atmospheric Inorganic Ions. *Sci. Total Environ.* **2017**, *580*, 1155–1161. https://doi.org/10.1016/j.scitotenv.2016.12.072.

(25) Bruland, K. W.; Lohan, M. C. 6.02 Controls of Trace Metals in Seawater. 25.

(26) Zhang, T.; Fiamingo, M.; Allen, H. C. Trace Metal Enrichment Driven by Phosphate Functional Group Binding Selectivity. *J. Geophys. Res. Oceans* **2018**, *123* (8), 5286–5297. https://doi.org/10.1029/2018JC013926.

(27) Barker, D. R.; Zeitlin, H. Metal-Ion Concentrations in Sea-Surface Microlayer and Size-Separated Atmospheric Aerosol Samples in Hawaii. *J. Geophys. Res. 1896-1977* **1972**, *77* (27), 5076–5086. https://doi.org/10.1029/JC077i027p05076.

(28) Adams, E. M.; Wellen, B. A.; Thiraux, R.; Reddy, S. K.; Vidalis, A. S.; Paesani, F.; Allen, H. C. Sodium–Carboxylate Contact Ion Pair Formation Induces Stabilization of Palmitic Acid Monolayers at High PH. *Phys. Chem. Chem. Phys.* **2017**, *19* (16), 10481–10490. https://doi.org/10.1039/C7CP00167C.

(29) Zhang, Z.; Liu, L.; Liu, C.; Cai, W. Studies on the Sea Surface Microlayer: II. The Layer of Sudden Change of Physical and Chemical Properties. *J. Colloid Interface Sci.* **2003**, *264* (1), 148–159. https://doi.org/10.1016/S0021-9797(03)00390-4.

(30) Adams, E. M.; Verreault, D.; Jayarathne, T.; Cochran, R. E.; Stone, E. A.; Allen, H. C. Surface Organization of a DPPC Monolayer on Concentrated $SrCl_2$ and $ZnCl_2$ Solutions. *Phys. Chem. Chem. Phys.* **2016**, *18* (47), 32345–32357. https://doi.org/10.1039/C6CP06887A.

(31) Li, S.; Du, L.; Tsona, N. T.; Wang, W. The Interaction of Trace Heavy Metal with Lipid Monolayer in the Sea Surface Microlayer. *Chemosphere* **2018**, *196*, 323–330. https://doi.org/10.1016/j.chemosphere.2017.12.157.

(32) Simon-Kutscher, J.; Gericke, A.; Hühnerfuss, H. Effect of Bivalent Ba, Cu, Ni, and Zn Cations on the Structure of Octadecanoic Acid Monolayers at the Air−Water Interface As Determined by External Infrared Reflection−Absorption Spectroscopy. *Langmuir* **1996**, *12* (4), 1027–1034. https://doi.org/10.1021/la950731q.

(33) Kumar, N.; Wang, L.; Siretanu, I.; Duits, M.; Mugele, F. Salt Dependent Stability of Stearic Acid Langmuir–Blodgett Films Exposed to Aqueous Electrolytes. *Langmuir* **2013**, *29* (17), 5150–5159. https://doi.org/10.1021/la400615j.

(34) Ebling, A. M.; Landing, W. M. Sampling and Analysis of the Sea Surface Microlayer for Dissolved and Particulate Trace Elements. *Mar. Chem.* **2015**, *177*, 134–142. https://doi.org/10.1016/j.marchem.2015.03.012.

(35) Gaines, G. L. *Insoluble Monolayers at Liquid-Gas Interfaces*; Interscience Publishers: New York, 1966.

(36) T. Buffeteau; B. Desbat; D. Eyquem. Attenuated Total Reflection Fourier Transform Infrared Microspectroscopy: Theory and Application to Polymer Samples. *Vib. Spectrosc.* **1996**, *11* (1), 29–36. https://doi.org/10.1016/0924-2031(95)00054-2.

(37) Flach, C. R.; Gericke, A.; Mendelsohn, R. Quantitative Determination of Molecular Chain Tilt Angles in Monolayer Films at the Air/Water Interface: Infrared Reflection/Absorption Spectroscopy of Behenic Acid Methyl Ester. *J. Phys. Chem. B* **1997**, *101* (1), 58–65. https://doi.org/10.1021/jp962288d.

(38) Gericke, A.; Huehnerfuss, H. In Situ Investigation of Saturated Long-Chain Fatty Acids at the Air/Water Interface by External Infrared Reflection-Absorption Spectrometry. *J. Phys. Chem.* **1993**, *97* (49), 12899–12908. https://doi.org/10.1021/j100151a044.

(39) Mendelsohn, R.; Brauner, J. W.; Gericke, A. External Infrared Reflection Absorption Spectrometry of Monolayer Films at the Air-Water Interface. *Annu. Rev. Phys. Chem.* **1995**, *46* (1), 305–334. https://doi.org/10.1146/annurev.pc.46.100195.001513.

(40) Mendelsohn, R.; Mao, G.; Flach, C. R. Infrared Reflection–Absorption Spectroscopy: Principles and Applications to Lipid–Protein Interaction in Langmuir Films. *Biochim. Biophys. Acta BBA - Biomembr.* **2010**, *1798* (4), 788–800. https://doi.org/10.1016/j.bbamem.2009.11.024.

(41) Shanmukh, S.; Biswas, N.; Waring, A. J.; Walther, F. J.; Wang, Z.; Chang, Y.; Notter, R. H.; Dluhy, R. A. Structure and Properties of Phospholipid–Peptide Monolayers Containing Monomeric SP-B1–25: II. Peptide Conformation by Infrared Spectroscopy. *Biophys. Chem.* **2005**, *113* (3), 233–244. https://doi.org/10.1016/j.bpc.2004.09.009.

(42) Wang, Y.; Du, X.; Guo, L.; Liu, H. Chain Orientation and Headgroup Structure in Langmuir Monolayers of Stearic Acid and Metal Stearate (Ag, Co, Zn, and Pb) Studied by Infrared Reflection-Absorption Spectroscopy. *J. Chem. Phys.* **2006**, *124* (13), 134706. https://doi.org/10.1063/1.2185629.

(43) Blume, A.; Kerth, A. Peptide and Protein Binding to Lipid Monolayers Studied by FT-IRRA Spectroscopy. *Biochim. Biophys. Acta BBA - Biomembr.* **2013**, *1828* (10), 2294–2305. https://doi.org/10.1016/j.bbamem.2013.04.014.

(44) William E. Wallace. Water. In *NIST Standard Reference Database Number 69*; NIST Chemistry WebBook; National Institute of Standards and Technology: Gaithersburg MD.

(45) Chattoraj, D. K.; Birdi, K. S. Spread Monolayer. In *Adsorption and the Gibbs Surface Excess*; Chattoraj, D. K., Birdi, K. S., Eds.; Springer US: Boston, MA, 1984; pp 179–232. https://doi.org/10.1007/978-1-4615-8333-2_6.

(46) Li, S.; Du, L.; Zhang, Q.; Wang, W. Stabilizing Mixed Fatty Acid and Phthalate Ester Monolayer on Artificial Seawater. *Environ. Pollut. Barking Essex 1987* **2018**, *242* (Pt A), 626–633. https://doi.org/10.1016/j.envpol.2018.07.043.

(47) Kartashynska, E. S.; Vysotsky, Y. B.; Vollhardt, D.; Fainerman, V. B.; Zakharov, A. Yu. Theoretical Description of Mixed Film Formation at the Air/Water Interface: Carboxylic Acids–Alcohols. *ACS Omega* **2018**, *3* (12), 16693–16705. https://doi.org/10.1021/acsomega.8b02583.

(48) Panda, A. K.; Nag, K.; Harbottle, R. R.; Possmayer, F.; Petersen, N. O. Thermodynamic Studies on Mixed Molecular Langmuir Films: Part 2. Mutual Mixing of DPPC and Bovine Lung Surfactant Extract with Long-Chain Fatty Acids. *Colloids Surf. Physicochem. Eng. Asp.* **2004**, *247* (1), 9–17. https://doi.org/10.1016/j.colsurfa.2004.07.008.

(49) Seoane, R.; Miñones, J.; Conde, O.; Miñones, J.; Casas, M.; Iribarnegaray, E. Thermodynamic and Brewster Angle Microscopy Studies of Fatty Acid/Cholesterol Mixtures at the Air/Water Interface. *J. Phys. Chem. B* **2000**, *104* (32), 7735–7744. https://doi.org/10.1021/jp001133+.

(50) Denton, J. K.; Kelleher, P. J.; Johnson, M. A.; Baer, M. D.; Kathmann, S. M.; Mundy, C. J.; Rudd, B. A. W.; Allen, H. C.; Choi, T. H.; Jordan, K. D. Molecular-Level Origin of the Carboxylate Head Group Response to Divalent Metal Ion Complexation at the Air–Water Interface. *Proc. Natl. Acad. Sci.* **2019**, *116* (30), 14874–14880. https://doi.org/10.1073/pnas.1818600116.

(51) Rudd, B. A. W.; Vidalis, A. S.; Allen, H. C. Thermodynamic versus Non-Equilibrium Stability of Palmitic Acid Monolayers in Calcium-Enriched Sea Spray Aerosol Proxy Systems. *Phys. Chem. Chem. Phys.* **2018**, *20* (24), 16320–16332. https://doi.org/10.1039/C8CP01188E.

(52) Zhang, T.; Brantley, S. L.; Verreault, D.; Dhankani, R.; Corcelli, S. A.; Allen, H. C. Effect of PH and Salt on Surface PKa of Phosphatidic Acid Monolayers. *Langmuir* **2018**, *34* (1), 530–539. https://doi.org/10.1021/acs.langmuir.7b03579.

(53) Adams, E. M.; Casper, C. B.; Allen, H. C. Effect of Cation Enrichment on Dipalmitoylphosphatidylcholine (DPPC) Monolayers at the Air-Water Interface. *J. Colloid Interface Sci.* **2016**, *478*, 353–364. https://doi.org/10.1016/j.jcis.2016.06.016.

(54) Wolstenholme, G. A.; Schulman, J. H. Metal-Monolayer Interactions in Aqueous Systems. Part I.—The Interaction of Monolayers of Long-Chain Polar Compounds with Metal Ions in the Underlying Solution. *Trans. Faraday Soc.* **1950**, *46* (0), 475–487. https://doi.org/10.1039/TF9504600475.

(55) Lee, Y.-L.; Yang, Y.-C.; Shen, Y.-J. Monolayer Characteristics of Mixed Octadecylamine and Stearic Acid at the Air/Water Interface. *J. Phys. Chem. B* **2005**, *109* (10), 4662–4667. https://doi.org/10.1021/jp045251z.

(56) Pfrang, C.; Rastogi, K.; Cabrera-Martinez, E. R.; Seddon, A. M.; Dicko, C.; Labrador, A.; Plivelic, T. S.; Cowieson, N.; Squires, A. M. Complex Three-Dimensional Self-Assembly in Proxies for Atmospheric Aerosols. *Nat. Commun.* **2017**, *8*. https://doi.org/10.1038/s41467-017-01918-1.

(57) Neumann, V.; Gericke, A.; Huehnerfuss, H. Comparison of Enantiomeric and Racemic Monolayers of 2-Hydroxyhexadecanoic Acid by External Infrared Reflection-Absorption Spectroscopy. *Langmuir* **1995**, *11* (6), 2206–2212. https://doi.org/10.1021/la00006a058.

(58) Cameron, D. G.; Casal, H. L.; Gudgin, E. F.; Mantsch, H. H. The Gel Phase of Dipalmitoyl Phosphatidylcholine. An Infrared Characterization of the Acyl Chain Packing. *Biochim. Biophys. Acta BBA - Biomembr.* **1980**, *596* (3), 463–467. https://doi.org/10.1016/0005-2736(80)90135-2.

(59) Schaefer, C. E.; Culina, V.; Nguyen, D.; Field, J. Uptake of Poly- and Perfluoroalkyl Substances at the Air–Water Interface. *Environ. Sci. Technol.* **2019**, *53* (21), 12442–12448. https://doi.org/10.1021/acs.est.9b04008.

(60) Khayyun, T. S.; Mseer, A. H. Comparison of the Experimental Results with the Langmuir and Freundlich Models for Copper Removal on Limestone Adsorbent. *Appl. Water Sci.* **2019**, *9* (8), 170. https://doi.org/10.1007/s13201-019-1061-2.

(61) Soares, J. C.; Soares, A. C.; Pereira, P. A. R.; Rodrigues, V. da C.; Shimizu, F. M.; Melendez, M. E.; Neto, C. S.; Carvalho, A. L.; Leite, F. L.; Machado, S. A. S.; Oliveira, O. N. Adsorption According to the Langmuir–Freundlich Model Is the Detection Mechanism of the Antigen P53 for Early Diagnosis of Cancer. *Phys. Chem. Chem. Phys.* **2016**, *18* (12), 8412–8418. https://doi.org/10.1039/C5CP07121F.

(62) Langmuir, I. The Adsorption of Gases on Plane Surfaces of Glass, Mica, and Platinum. *J. Am. Chem. Soc.* **1918**, *40* (9), 1361–1403. https://doi.org/10.1021/ja02242a004.

(63) Henry, D. C. LX. *A Kinetic Theory of Adsorption*. *Lond. Edinb. Dublin Philos. Mag. J. Sci.* **1922**, *44* (262), 689–705. https://doi.org/10.1080/14786441108634035.

(64) Jeppu, G. P.; Clement, T. P. A Modified Langmuir-Freundlich Isotherm Model for Simulating PH-Dependent Adsorption Effects. *J. Contam. Hydrol.* **2012**, *129–130*, 46–53. https://doi.org/10.1016/j.jconhyd.2011.12.001.

(65) Pisarchick, M.L.; Thompson, N.L. Binding of a Monoclonal Antibody and Its Fab Fragment to Supported Phospholipid Monolayers Measured by Total Internal Reflection Fluorescence Microscopy. *Biophys. J.* **1990**, *58* (5), 1235–1249. https://doi.org/10.1016/S0006-3495(90)82464-4.

For Table of Contents Only